

Synthesis, characterization and catalytic performance of ZnO–CeO₂ nanoparticles in wet oxidation of wastewater containing chlorinated compounds

Anushree¹ · S. Kumar¹ · C. Sharma¹

Received: 26 June 2017 / Accepted: 11 September 2017 / Published online: 18 September 2017
© The Author(s) 2017. This article is an open access publication

Abstract Here we report the catalytic property of ZnO–CeO₂ nanoparticles towards oxidative degradation of organic pollutants present in industrial wastewater. The catalysts were prepared by co-precipitation method without using any surfactant. The physicochemical properties of catalysts were studied by XRD, Raman, XPS, N₂-sorption, FE-SEM, TEM and EDX techniques. The characterization results confirmed the formation of porous ZnO–CeO₂ nanocatalysts with high surface area, pore volume and oxygen vacancies. ZnO–CeO₂ nanocatalysts exhibited appreciable efficiency in CWAO of industrial wastewater under mild conditions. The Ce₄₀Zn₆₀ catalyst was found to be most efficient with 72% color, 64% chemical oxygen demand (COD) and 63% total organic carbon (TOC) removal. Efficient removal of chlorophenolics (CHPs, 59%) and adsorbable organic halides (AOX, 54%) indicated the feasibility of using ZnO–CeO₂ nanocatalysts in degradation of non-biodegradable and toxic chlorinated compounds.

Keywords ZnO–CeO₂ · Catalysis · Porous · Oxygen vacancy · Wet air oxidation

Introduction

The discharge of industrial wastewaters is continuously contaminating our water resources. The increasing environmental concerns have awakened industries to minimize the pollution load from wastewater. Various treatment methods have been studied to remove the pollutants from

industrial wastewater (Richardson 2007; Robinson et al. 2001). Catalytic wet air oxidation (CWAO) has received considerable interest, as it mineralizes the organic contaminants into biodegradable intermediates or innocuous compounds by utilizing the mild oxidant, i.e., air or oxygen. Various noble metals, metal oxides and their combinations have been extensively studied as heterogeneous catalysts in CWAO. Qin et al. (2001) investigated the noble metal catalysts (Pt, Pd, Ru) supported on Al₂O₃ or activated carbon for CWAO of p-chlorophenol. Complete conversion of p-CP and 97.9% TOC reduction was obtained with Pt/AC catalyst at 180 °C and 2.6 MPa. Pintar et al. (2001) studied the CWAO of acidic and alkaline kraft bleaching plant effluents over TiO₂, ZrO₂, Ru/TiO₂ and Ru/ZrO₂. Ru doped catalysts exhibited more than 99% TOC removal at 190 °C and 5.5 MPa. Xu et al. (2006) reported up to 93% COD removal during CWAO of phenol in presence of Cu_{0.5-x}Fe_xZn_{0.5}Al₂O₄. In spite of extensive research, the application of CWAO is limited due to severe operating conditions. Therefore, still there is the need of cost-effective, active and stable catalyst for CWAO of industrial wastewater under mild reaction conditions.

During CWAO, high temperature and pressure enhances the reaction rate and improves the oxygen solubility. Therefore, the catalyst with high reactivity and good oxygen buffering can serve as a suitable candidate. The rapid growth of nanotechnology offers great opportunity to develop the next-generation catalyst for wastewater treatment (Ghasemzadeh et al. 2014; Anjum et al. 2016). The high activity, mobility in solution, specific surface areas, stability and easy separation from reaction mixture, make them the ultimate candidate for catalysis (Khin et al. 2012; Xia et al. 2016). CeO₂ gained considerable attention as an oxidative catalyst due to its oxygen storage and release capacity (Gupta et al. 2010). The interaction of CeO₂ with

✉ Anushree
anushreejatrana@gmail.com

¹ Indian Institute of Technology Roorkee, Roorkee 247667, India

low valent element strongly enhances its redox property, which leads to the promoted oxidation efficiency (Anushree and Kumar 2015a; Arena 2014). We have selected ZnO–CeO₂ by taking its wide catalytic applications in consideration (Habibi and Fakhropor 2016; Faisal et al. 2011; Assal et al. 2017). Here we investigate the potential of ZnO–CeO₂ nanoparticles toward oxidative abatement of pollutants present in paper industry wastewater. The catalytic activity was evaluated for the removal of chemical oxygen demand (COD), biochemical oxygen demand (BOD₅), total organic carbon (TOC), adsorbable organic halides (AOX) and various chlorophenolic compounds (chlorophenols, chlorocatechols, chloroguaiacols, chlorovanilins, chlorosyringols, and chlorosyringaldehydes).

Experimental

Wastewater sample

The paper industry wastewater was collected from the outlet of primary clarifier. Paper industry wastewater is characterized by significant amounts of pollutants, including chlorinated compounds, fatty acids, tannins, stilbenes, resin acids, lignin and its derivatives, sulfur and its compounds, etc. (Vepsäläinen et al. 2011; Catalkaya and Kargi 2008). The chlorinated compounds present in the paper industry wastewater are toxic in nature and are collectively estimated as AOX. Some of the chlorinated compounds have been classified as priority pollutants by EPA, US (Kozak et al. 1979).

Materials and methods

The starting materials for catalyst preparation were of analytical grade. 1M H₂SO₄ solution was used to adjust the pH of wastewater. Chlorophenolics standards were obtained from Aldrich and Helix Biotech Corporation. Analytical grade acetic anhydride was used after double-distillation. Acetone/water (10:90) solution was used for the preparation of standard stock solution of individual chlorophenolics.

The physicochemical parameters of wastewater were determined according to standard APHA procedures (Clesceri et al. 1998). COD indicates the equivalent amount of oxygen, required to chemically oxidize the organic compounds in wastewater. It was measured by closed reflux titrimetric method, using a mixture of chromic (K₂Cr₂O₇) and sulfuric acids. BOD₅ measures the biodegradable fraction of organic load. It was determined by measuring the dissolved oxygen (DO) before and after incubation of samples at 20 °C for 5 days. TOC is the

amount of carbon found in organic load of wastewater. TOC values were determined through a TOC analyzer (TOC-L CPH, Shimadzu) based on catalytic combustion oxidation of organic carbon to CO₂. The analysis was carried out through the difference method, where the difference between total carbon (TC) and total inorganic carbon (IC) gave the TOC value. AOX indicates the amount of chlorinated compounds adsorbable to activated carbon. The AOX analyzer (Dextar, Thermo Electron Corporation) was based on combustion ion chromatography, where the electrochemical titration method was utilized for quantification of halogens as AOX. Color values were assessed by a UV–Vis spectrophotometer (SPEKOL 2000, Analytic Jena) at 465 nm. The values were calculated from the calibration curve made between absorbance and color units for different concentrations of standard Pt–Co solution. CHPs analysis was done by GC–MS (Trace GC Ultra DSQ, Thermo) furnished with a capillary column (TR-5). The procedure suggested by Lindstrom and Nordin (1976) was followed for the extraction of CHPs from wastewater. CHPs were first recognized by the NIST library and then retention times were verified by injecting the pure standard solutions (Choudhary et al. 2015).

Synthesis of catalysts

ZnO–CeO₂ nanocatalysts with Zn:Ce mole ratio of 80:20, 60:40, 50:50, 40:60 and 20:80 were prepared by a facile coprecipitation method. 1M Zn(NO₃)₂·6H₂O and Ce(NO₃)₃·6H₂O solutions were mixed according to specific ratios, and the solution was stirred at 70 °C for 15 min. 0.5M NaOH was added drop-wise to attain the pH value of 10. The resulting solution was stirred for 2 h and the washed precipitates were dried overnight at 110 °C to obtain the hydroxide precursors. The oxides were obtained after calcination of these hydroxide precursors at 400 °C for 4 h under air atmosphere.

Characterization of catalysts

The catalysts were characterized by various spectroscopic and non-spectroscopic techniques. The phase identification was done by XRD (Bruker AXS D8) with Cu K α radiation ($\lambda = 0.15$ nm) as primary beam, at a scan rate of 2° min⁻¹. Diffraction patterns were compared with the JCPDS files. The crystallite size was assessed by X-ray line broadening from the Scherrer equation. FT-IR spectra of samples were recorded on a spectrophotometer (PerkinElmer, C91158) operating at a resolution of 4 cm⁻¹. XPS analysis was carried out on a spectrometer (ULVAC-PHI 5000 Versa Probe II) equipped with monochromatic Al-K α source ($h\nu = 1486.6$ eV). Raman spectra were recorded on a spectrometer (Renishaw Invia) at an excitation wavelength

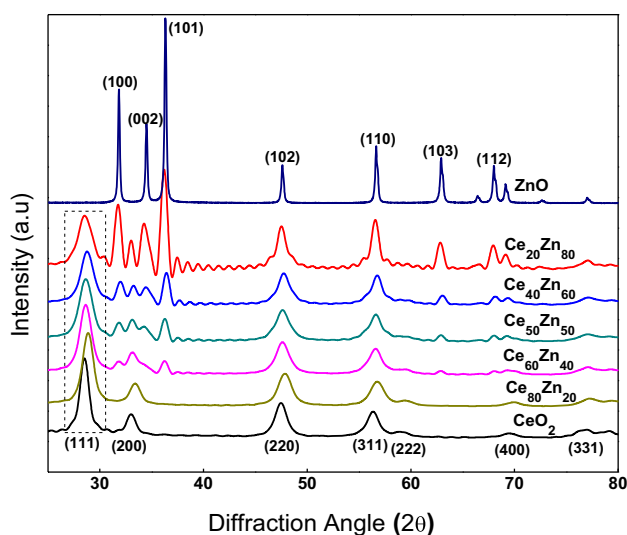


Fig. 1 XRD pattern of ZnO–CeO₂ catalysts

of 514 nm. N₂-sorption isotherms were recorded on a gas sorption analyzer (Quantachrome ASiQwin™). The specific surface area was calculated by BET equation and the pore size distribution (PSD) was determined by DFT, which were included in ASiQwin software. The morphology of samples was studied by FE-SEM (Quanta, 20 kV) and TEM (Tecnai G² STWIN, 200 kV). Elemental analysis of samples was carried out by EDX (51 XMX 1005 Oxford) coupled with FE-SEM microscope chamber.

Activity testing of catalysts

The oxidative degradation of organic pollutants in wastewater was carried out in a glass reactor at 1 atm, catalyst dose 1 g L⁻¹, pH 4, temperature 90 °C and reaction time 2 h (Anushree and Kumar 2015b). The wastewater and the weighed amount of catalyst were loaded into

the reactor followed by oxygen introduction through a gas inlet. After the experiment, the catalyst was recovered by centrifugal separation and the supernatant liquid was analyzed for various physicochemical parameters.

Results and discussion

XRD analysis

The diffraction pattern of catalysts are presented in Fig. 1. CeO₂ displayed the pattern of cubic phase with reflections at 2θ value of 28.5°, 33°, 47.4° and 56.3° corresponding to (111), (200), (220) and (311) crystal planes, respectively (JCPDS 81-0792) (Anushree and Kumar 2015b). ZnO exhibited the reflections for tetragonal phase at 31.8°, 34.5°, 36.3°, 47.6°, 56.7°, 63°, 66.5°, 68.1°, 69.2°, 72.8° and 77.2° corresponding to (100), (002), (101), (102), (110), (103), (200), (112), (201), (004) and (202) respectively (JCPDS 79-0205). There was no diffraction peak for ZnO up to zinc content of 20 mol%, indicating the incorporation of ZnO within ceria lattice. Further increase in Zn content exhibited the peaks for ZnO phase, indicating that a part of ZnO was inserted into the ceria lattice and another part was precipitated as a separate phase onto CeO₂ surface. The broader and less intense peaks for ZnO–CeO₂ indicated the decreased crystallite size. The crystallite size, lattice parameters estimated from the broadening of (111) and (101) diffraction of CeO₂ and ZnO are listed in Table 1.

The crystallite size of CeO₂ was significantly decreased with increase in Zn content. This decrease indicated the role of Zn²⁺ towards inhibition of CeO₂ crystal growth, which is consistent with the previous report (Lin et al. 2015a). The lattice parameter of CeO₂ was found to be 5.417 Å, which decreased to 5.357 Å for Ce₈₀Zn₂₀. The

Table 1 Properties of ZnO–CeO₂ catalysts

Sample	Crystallite size (nm) ^a CeO ₂	Lattice parameter (Å) ^a	Average aggregate size (nm) ^b	Specific surface area (m ² /g) ^c	Total pore volume (m ³ /g) ^c
CeO ₂	10.6	5.417	45 ± 1.4	20	0.089
Ce ₈₀ Zn ₂₀	6.8	5.357	41 ± 1.7	54	0.204
Ce ₆₀ Zn ₄₀	6.2	5.382	30 ± 5.4	65	0.105
Ce ₅₀ Zn ₅₀	6.1	5.387	18 ± 2.3	90	0.110
Ce ₄₀ Zn ₆₀	5.6	5.373	16 ± 2.1	104	0.247
Ce ₂₀ Zn ₈₀	5.3	5.393	18 ± 0.9	106	0.202
ZnO	–	–	40 ± 1.9	35	0.164

^a XRD

^b FE-SEM micrographs

^c N₂-sorption

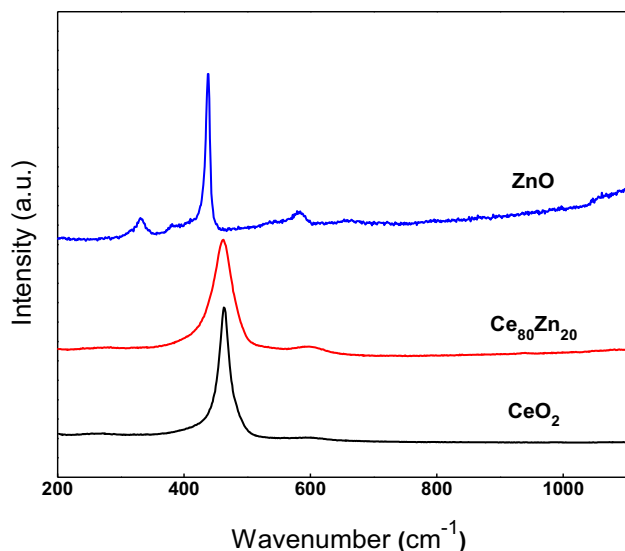
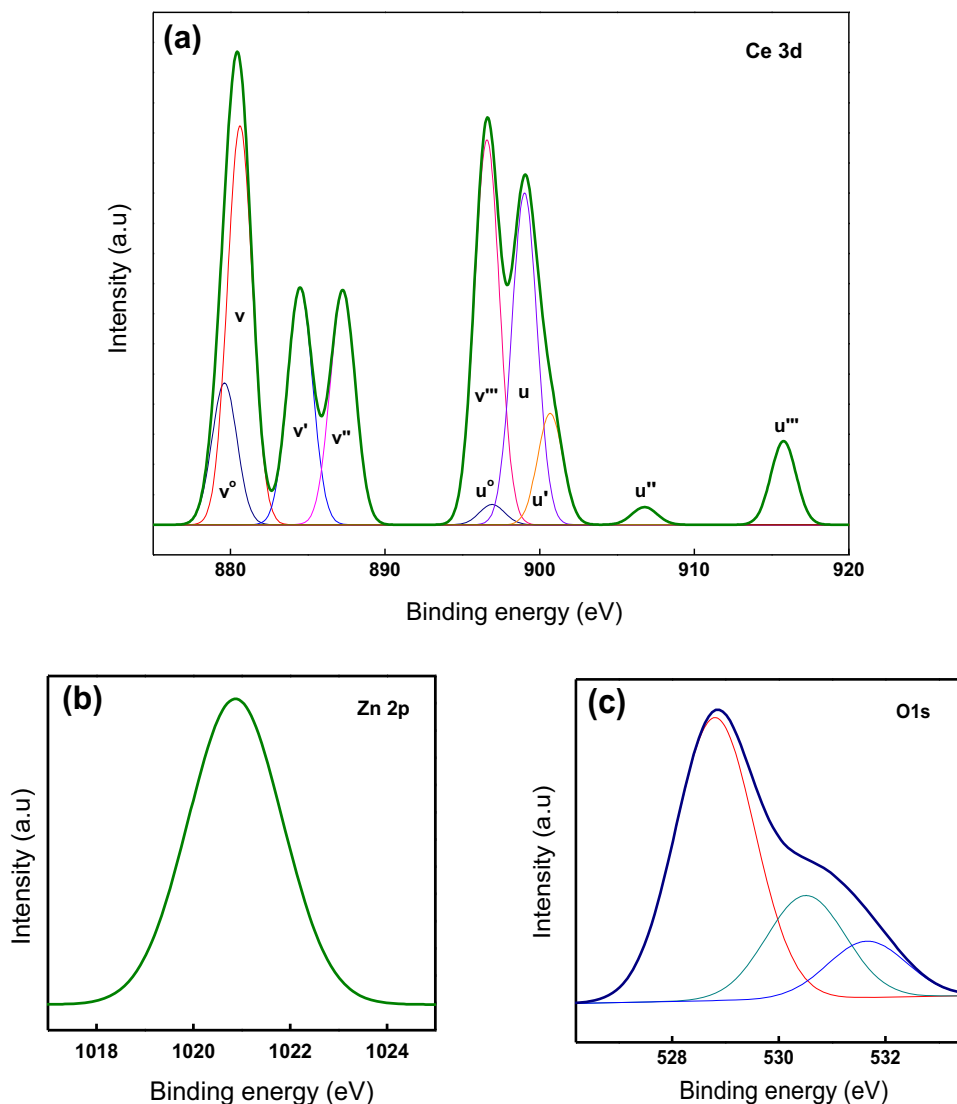


Fig. 2 Raman spectra of catalysts

Fig. 3 XPS spectra of $\text{Ce}_{40}\text{Zn}_{60}$ catalyst **a** Ce 3d, **b** Zn 2p, **c** O 1s



overall trend of decrease in lattice parameter is in good correlation with the experimental study by Ramasamy and Vijayalakshmi (2015). The decreased lattice parameter can be ascribed to the smaller ionic radius of Zn^{2+} in comparison to Ce^{4+} (Le Gal and Abanades 2012).

Raman analysis

Raman spectroscopy was carried out to understand the structural changes in CeO_2 nanocrystals due to Zn addition, and to characterize the oxygen vacancies (Fig. 2). CeO_2 nanoparticles exhibited a strong peak at 462 cm^{-1} , corresponding to symmetric breathing mode (F_{2g}) of oxygen in fluorite structure of CeO_2 (Jha et al. 2016). The $\text{Ce}_{80}\text{Zn}_{20}$ nanocatalyst exhibited an additional band at 600 cm^{-1} , related to the oxygen vacancies due to the presence of Ce^{3+} in CeO_2 lattice (Lin et al. 2015b). The intensity ratio of the bands at 600 and 462 cm^{-1} (I_{600}/I_{462}) was found to be 0.07,

Fig. 4 **a** N_2 -sorption isotherms; **b** pore size distribution of $Ce_{40}Zn_{60}$ nanocatalyst

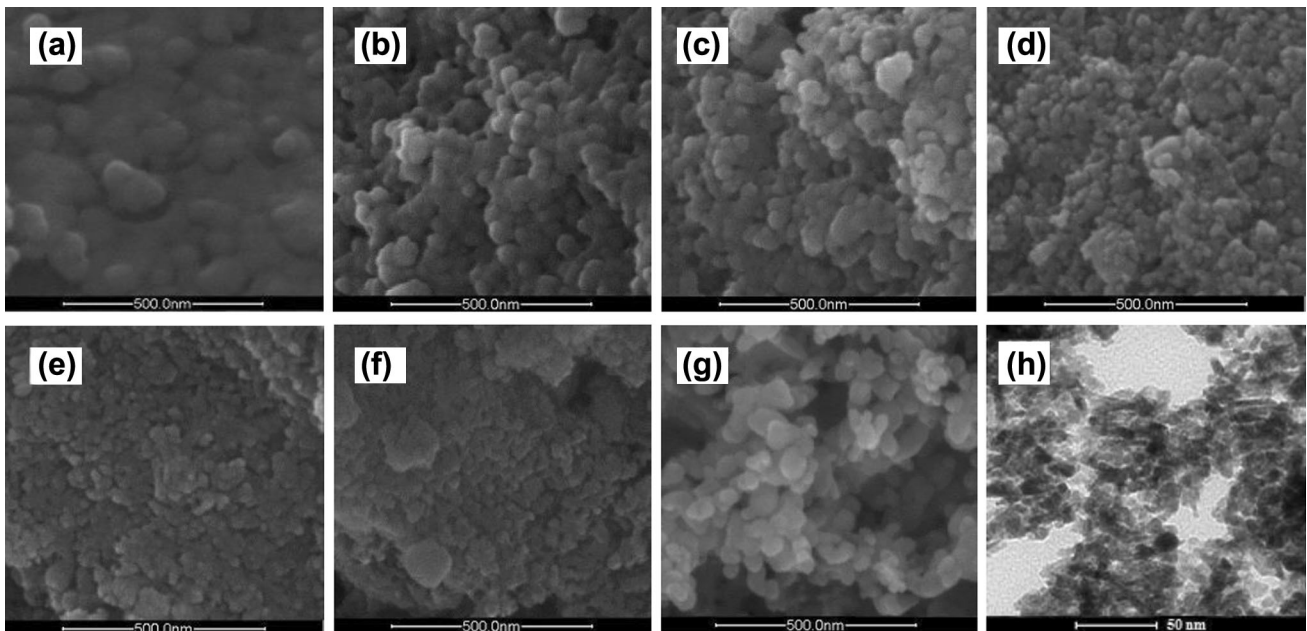
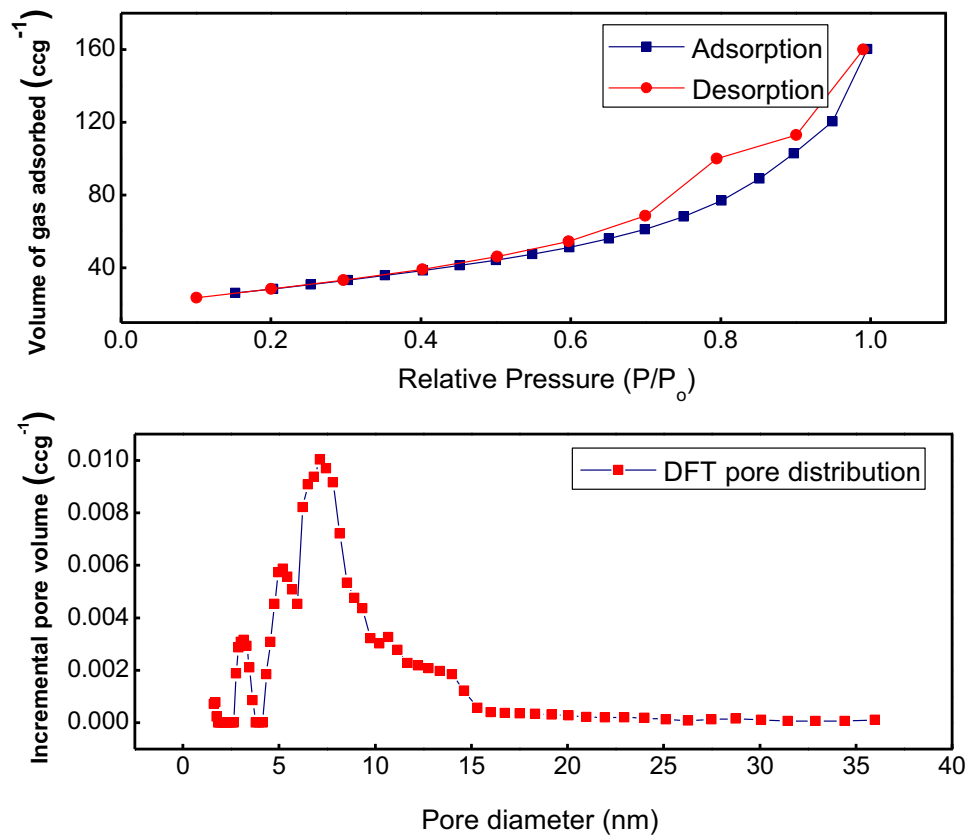


Fig. 5 FE-SEM micrographs of **a** CeO_2 , **b** $Ce_{80}Zn_{20}$, **c** $Ce_{60}Zn_{40}$, **d** $Ce_{50}Zn_{50}$, **e** $Ce_{40}Zn_{60}$, **f** $Ce_{20}Zn_{80}$, **g** ZnO , **h** TEM micrograph of $Ce_{40}Zn_{60}$

which is in good correlation with the previous study (Bao et al. 2008). ZnO exhibited the bands at 330 cm^{-1} (E_2 high- E_2 low), 437 cm^{-1} (E_2 high), and 658 cm^{-1} (E_2

low + B_1 high). Small peaks at 380 and 583 cm^{-1} were the characteristics of high density of common oxygen defects in ZnO (Pal et al. 2014). On the basis of Raman

spectroscopy, it can be concluded that zinc doping introduces oxygen vacancies into the CeO_2 lattice.

XPS analysis

The oxidation states of metal ions in $\text{Ce}_{40}\text{Zn}_{60}$ nanocatalyst were investigated by XPS analysis. Figure 3 depicts the Ce 3*d*, Zn 2*p* and O 1*s* XPS spectra deconvoluted using a peak fitting process. Ce 3*d* XPS spectra exhibited eight fitted peaks with two multiplets (*u* and *v*) corresponding to 3*d*_{5/2} and 3*d*_{3/2} spin-orbital components (Burroughs et al. 1976). Six main components characteristic of Ce^{4+} were observed at the binding energies of 880.6, 887.3, 896.5, 899, 906.7 and 915.7 eV corresponding to *v*, *v'*, *v''*, *u*, *u'* and *u''*, respectively. Peaks for *v*^o (879.6 eV), *v'* (884.4 eV), *u*^o (879 eV) and *u'* (900.7 eV) components evidenced the presence of Ce^{3+} (Bera and Anandan 2014).

Atomic fraction of Ce^{3+} calculated from the integrated peak areas ratio of Ce^{3+} to the total of Ce^{4+} and Ce^{3+} (Babu et al. 2009), was found to be 26%. Zn 2*p*_{3/2} spectra presented a peak at 1020.9, corresponding to the presence of Zn^{2+} in ZnO lattice (Das and Mondal 2014). O 1*s* spectra exhibited three peaks. First peak centered at 528.8 eV was related to the structural/lattice oxygen (63.9%). Peak at 531.6 eV indicated the presence of adsorbed surface oxygen as OH ions (12.7%). The additional peak at 530.5 eV was related to the supercharged oxygen (O_2^-) near oxygen vacant sites at the surface (23.3%). This particular peak evidenced the oxygen storage/release capacity of the nanocatalyst (Kullgren et al. 2013).

N_2 -sorption analysis

The surface area and porosity of catalysts was investigated by N_2 -sorption measurements and the related BET surface area and pore volume of all catalysts are summarized in Table 1. All ZnO– CeO_2 catalysts exhibited higher surface than the single metal oxides, which increased from 54 to 106 m²/g with the increasing Zn content. This increase can be related to the decreased crystallite size, as indicated by XRD. Figure 4a presents the adsorption–desorption isotherm of $\text{Ce}_{40}\text{Zn}_{60}$ catalyst, where the presence of hysteresis loop indicated the presence of mesopores. During adsorption, the inflection was observed at high relative pressure, which represents the capillary condensation of nitrogen during the filling of secondary pores. The desorption isotherm resulted into a narrow hysteresis at $P/P_0 > 0.5$, indicating the irregular pore structure (Anushree and Kumar 2016). It is evident from isotherm that the aggregation of non-porous primary spherical particles resulted into the secondary pores (Hannach et al. 2014). Pore size distribution, confirmed the presence of disordered mesopores, with size ranging from 3 to 7 nm (Fig. 4b).

FE-SEM and TEM analysis

Figure 5a–g presents the FE-SEM micrograph of catalysts, and the aggregate size ranges assessed from micrographs are reported in Table 1. The CeO_2 particles were aggregated in the average size of 45 nm. With increasing Zn content the aggregate size was considerably decreased and achieved the minimum value of around 16 nm. TEM micrograph of $\text{Ce}_{40}\text{Cu}_{60}$ along with its SAED pattern is shown in Fig. 5h. TEM micrograph clearly revealed the presence of mesopores, formed by aggregation of particles. Estimated from figure, the average particle size of $\text{Ce}_{40}\text{Zn}_{60}$ was found to be 6 nm, which is in accordance with XRD results.

Catalytic activity studies

Wastewater was analyzed for various physicochemical parameters, i.e., COD, BOD, color, AOX, TOC, CHPs, and their average values are listed in Table 2. The average value of COD, Color, AOX and TOC removal in presence of ZnO– CeO_2 nanocatalysts is presented in Fig. 6. CeO_2

Table 2 Average value of physicochemical parameters of wastewater

Parameter	Value
COD (mg L ⁻¹)	914
BOD ₅ (mg L ⁻¹)	242
TOC (mg L ⁻¹)	188
Color (mg Pt–Co L ⁻¹)	3004
AOX (mg L ⁻¹)	17.4
CHPs (μg L ⁻¹)	472
BOD ₅ /COD	0.264

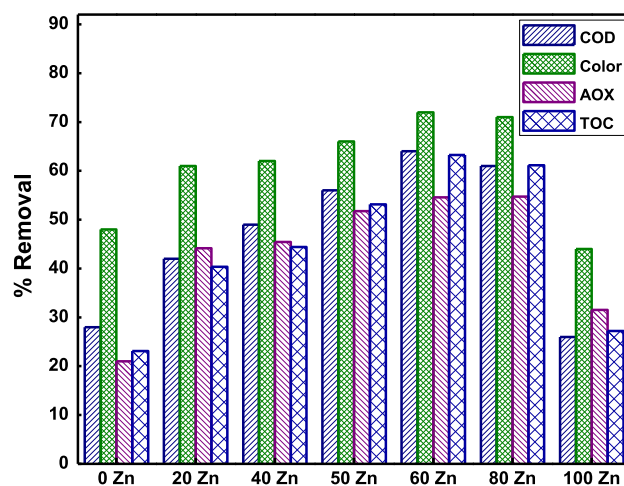


Fig. 6 Average COD, color, AOX and TOC removal

Table 3 Average concentration of CHPs in paper industry wastewater before and after CWAO

S. no.	Name of compound	Before	After	% Removal
1.	3-CP	14.5	11.9	17
2.	4-CP	5.9	5.1	15
3.	2,6-DCP	29.9	18.3	39
4.	2,5-DCP	78.8	34.4	56
5.	2,4-DCP	33.4	14.6	56
6.	3,4-DCP	0.3	0.2	30
7.	2,3-DCP	0.2	ND	100
8.	2,4,5-TCP	212.7	55.3	74
10.	2,3,5-TCP	3.6	1.5	58
11.	2,4,6-TCP	0.08	ND	100
12.	2,3,4-TCP	1.4	0.8	40
13.	PCP	0.2	ND	100
14.	4-CG	41.9	24.6	41
15.	4,5-DCG	41.6	22.1	47
16.	4,6-DCG	0.5	0.5	3
17.	3,4,6-TCG	0.3	0.8	36
18.	3,4,5-TCG	0.1	0.06	31
19.	4,5,6-TCG	0.3	0.1	58
20.	TeCG	0.4	0.3	32
22.	3,5-DCC	3.6	2.8	22
24.	TCS	1.2	0.5	54
25.	2,6-DCSA	1.0	ND	100
Total		471.9	193.3	59

ND not detected

exhibited the low abatement profile with 48% color, 28% COD, 23% TOC and 21% AOX removal. Addition of ZnO increased the catalyst activity, with maximum removal of 64% COD, 72% color, 54% AOX and 63% TOC over $Ce_{40}Zn_{60}$ catalyst. Paper industry wastewater presented a low Biodegradability index ($BI = BOD_5/COD$) of 0.264 which was enhanced up to 0.423 after CWAO in presence of $Ce_{40}Zn_{60}$ nanocatalyst. According to earlier reports a BI

value of 0.4 is required for the complete biodegradation of wastewater (Chamarro et al. 2001). Thus, CWAO was efficient in converting the non-biodegradable compounds into easily biodegradable compounds. The treatment efficiency of $Ce_{40}Zn_{60}$ nanocatalyst was further established for the chlorophenolics (CHPs) removal. GC–MS analysis (Table 3) of wastewater indicated the presence of total 25 CHPs. These compounds were categorized as chlorophenols (CP), chloroguaiacols (CG), chlorocatechols (CC), chlorosyringols (CS) and chlorosyringaldehydes (CSA), according to their chemical family. Out of these CP contributed the highest portion of 80.75%, followed by CG (18.03%), CC (0.77%), CS (0.25%) and CSA (0.21%) (Fig. 7a). Based on chlorine atom substitution (Fig. 7b), CHPs were classified as mono-chlorophenolics (MCHPs, 13.21%), di-chlorophenolics (DCHPs, 40.21%), tri-chlorophenolics (TCHPs, 46.54%), tetra-chlorophenolics (TeCHPs, 0.01%) and penta-chlorophenolics (PCHPs, 0.05%). Overall 59% removal of CHPs was attained after CWAO, with 62.7% CP, 43.9% CG, 22.1% CC, 54.1% CS and 100% CSA removal (Fig. 8a). The PCHPs removal was 100%, followed by TCHPs (73.3%), DCHPs (38%), MCHPs (33.2%) and TeCHPs (32.3%) (Fig. 8b). Moreover, 2,3-DCP, 2,6-DCSA, 2,4,6-TCP and PCP were not detected after treatment, indicating their complete degradation during CWAO.

Recently, Ovejero et al. (2007) investigated the CWAO of phenol over Platinum supported on multiwalled carbon nanotubes (MWCNTs), and reported 94% phenol and 80% TOC conversion at 2 MPa and 200 °C. Yang et al. (2015) reported complete removal of phenol at 155 °C and 2.5 MPa over MWCNTs functionalized by O_3 . Morales-Torres et al. (2011) tested the Pt/ACs in CWAO of aniline, and achieved complete removal at 200 °C and 5 MPa. In present study, 64% COD, 72% color, 63% TOC, 54% AOX and 59% CHPs removal was obtained during CWAO of paper industry wastewater over $Ce_{40}Zn_{60}$ nanocatalyst at 90 °C and 0.1 MPa (1 atm). Also, there was an appreciable increase in BI from 0.264 to 0.423. Therefore, the mild

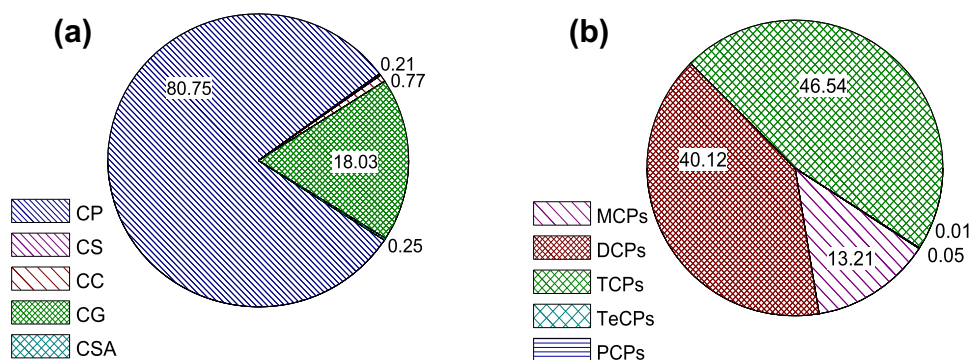
Fig. 7 Percentage of CHPs in wastewater, according to **a** chemical family, **b** attached chlorine atom

Fig. 8 Percent removal of CHPs over $Ce_{40}Zn_{60}$ catalyst, according to **a** chemical family, **b** attached chlorine atom

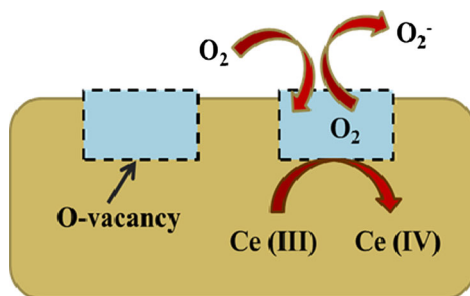
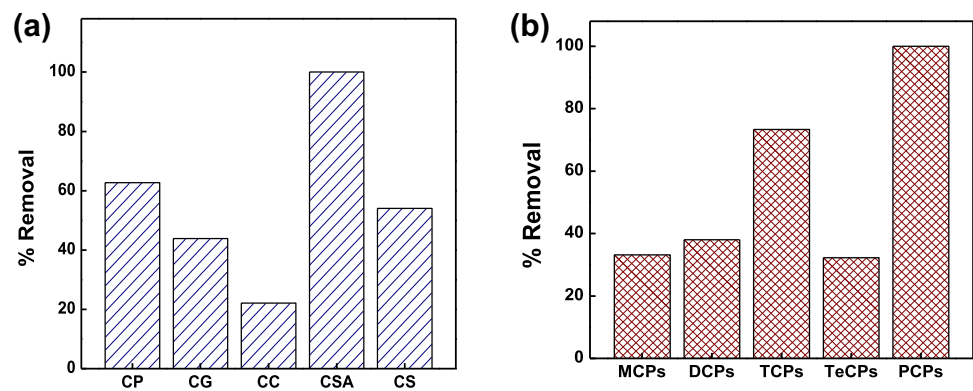


Fig. 9 Schematic diagram for oxygen buffering capacity of ZnO–CeO₂

experimental conditions tried in our study seem to be advantageous.

Role of catalyst in CWAO

Based upon above characterization results and the mechanisms suggested in literature (Moreno et al. 2010), it could be concluded that Ce^{4+} is easily reduced to Ce^{3+} , which is the main active site. The reactant is adsorbed to the catalyst surface and gets oxidized by the interface lattice oxygen, generating oxygen vacancy at the interface. Next, the gaseous O_2 fills up the oxygen vacancy, forming adsorbed active oxygen species which can react with another reactant molecule. Figure 9 gives a graphical presentation to the role of ZnO–CeO₂ catalyst in CWAO.

Conclusion

The ZnO–CeO₂ nanocatalysts prepared by the co-precipitation method exhibited good performance in CWAO of paper industry wastewater under mild conditions. Physicochemical characterizations of catalysts depicted the favourable role of Zn in textural and structural modifications of CeO₂. Catalytic activity was improved by the complementary effect between zinc and ceria. The combination of CeO₂ and ZnO in 40:60 molar ratios allowed

the highest removal efficiency. Presence of oxygen vacancies, small size of particles, high surface area and high pore volume justified the efficiency of ZnO–CeO₂ nanocatalysts in removal of organic pollutants.

Acknowledgements The research grant for this study provided by MHRD, Government of India, is gratefully acknowledged. The authors also thank Dr. Vive Kumar (CRDT, Indian Institute of Technology, Delhi) for his help in preparing the revised form of the manuscript.

Open Access This article is distributed under the terms of the Creative Commons Attribution 4.0 International License (<http://creativecommons.org/licenses/by/4.0/>), which permits unrestricted use, distribution, and reproduction in any medium, provided you give appropriate credit to the original author(s) and the source, provide a link to the Creative Commons license, and indicate if changes were made.

References

- Anjum M, Miandad R, Waqas M, Gehany F, Barakat MA (2016) Remediation of wastewater using various nano-materials, Arab. J Chem. doi:10.1016/j.arabj.2016.10.004
- Anushree S, Kumar C (2015a) Sharma, NiO–CeO₂ nano-catalysts: Synthesis, characterization and application in catalytic wet air oxidation of wastewater. Mater. Express 5:419–428
- Anushree S, Kumar C (2015b) Sharma, Synthesis, characterization and catalytic wet air oxidation property of mesoporous Ce_{1-x}Fe_xO₂ mixed oxides. Mater. Chem. Phys. 155:223–231
- Anushree S, Kumar C (2016) Sharma, Ce_{1-x}Co_xO_y nanocatalysts: synthesis, characterization and environmental application. Catal Sci Technol 6:2101–2111
- Arena F (2014) Multipurpose composite MnCeO_x catalysts for environmental applications. Catal Sci Technol 4:1890–1898
- Assal ME, Kuniyil M, Shaik MR, Khan M, Al-Warthan A, Siddiqui MRH, Adil SF (2017) Synthesis, characterization, and relative study on the catalytic activity of zinc oxide nanoparticles doped MnCO₃–MnO₂, and –Mn₂O₃ nanocomposites for aerial oxidation of alcohols. J Chem. doi:10.1155/2017/2937108
- Babu S, Thanneer R, Inerbaev T, Day R, Masunov AE, Schulte A, Seal S (2009) Dopant-mediated oxygen vacancy tuning in ceria nanoparticles. Nanotechnology 20:085713–085717

- Bao H, Chen X, Fang J, Jiang Z, Huang W (2008) Structure-activity relation of $\text{Fe}_2\text{O}_3\text{-CeO}_2$ composite catalysts in CO oxidation. *Catal Lett* 125:160–167
- Bera P, Anandan C (2014) XRD and XPS studies of room temperature spontaneous interfacial reaction of CeO_2 thin films on Si and Si_3N_4 substrates. *RSC Adv* 4:62935–62939
- Burroughs A, Hamnett A, Orchard F, Thornton G (1976) Satellite structure in the X-ray photoelectron spectra of some binary and mixed oxides of lanthanum and cerium. *J Chem Soc Dalton Trans* 17:1686–1698
- Catalkaya EC, Kargi F (2008) Advanced oxidation treatment of pulp mill effluent for TOC and toxicity removals. *J Environ Manag* 87:396–404
- Chamarro E, Marco A, Esplugas S (2001) Use of Fenton reagent to improve the biodegradability of effluents. *Water Res* 35:1047–1051
- Choudhary AK, Kumar S, Sharma C (2015) Removal of chloroorganics and color from pulp and paper mill wastewater by polyaluminium chloride as coagulant. *Desalin Water Treat* 53:697–708
- Clesceri LS, Greenberg AE, Eaton AD (1998) Standard methods for the examination of water and wastewater, 20th edn. American Public Health Association, Washington
- Das D, Mondal P (2014) Photoluminescence phenomena prevailing in *c*-axis oriented intrinsic ZnO thin films prepared by RF magnetron sputtering. *RSC Adv* 4:35735–35743
- Faisal M, Khan SB, Rahman MM, Jamal A, Akhtar K, Abdullah MM (2011) Role of ZnO– CeO_2 nanostructures as a photo-catalyst and chemi-sensor. *J Mater Sci Technol* 27:594–600
- Ghasemzadeh G, Momenpour M, Omid F, Hosseini MR, Ahani M, Barzegari A (2014) Applications of nanomaterials in water treatment and environmental remediation. *Front Environ Sci Eng* 8:471–482
- Gupta A, Waghmare UV, Hegde MS (2010) Correlation of oxygen storage capacity and structural distortion in transition-metal-, noble-metal-, and rare-earth-ion-substituted CeO_2 from first principles calculation. *Chem Mater* 22:5184–5198
- Habibi MH, Fakhropor M (2016) Preparation of cerium zinc oxide nanocomposite derived by hydrothermal route coated on glass and its application in water treatment. *Desalin Water Treat* 57:26204–26210
- Hannach ME, Soboleva T, Malek K, Franco AA, Prat M, Pauchet J, Holdcroft S (2014) Characterization of pore network structure in catalyst layers of polymer electrolyte fuel cells. *J Power Sour* 247:322–326
- Jha A, Jeong DW, Lee YL, Jang WJ, Shim JO, Jeon KW, Rode CV, Roh HS (2016) Chromium free high temperature water-gas shift catalyst for the production of hydrogen from waste derived synthesis gas. *Appl Catal A Gen* 522:21–31
- Khin MM, Nair AS, Babu VJ, Murugana R, Ramakrishna S (2012) A review of nanomaterials for environmental remediation. *Energy Environ Sci* 5:8075–8109
- Kozak VP, Simsiman GV, Chesters G, Stensby D, Harkin J (1979) Reviews of the environmental effects of pollutants: XI. Chlorophenols, Washington, DC, US Environmental Protection Agency, (EPA 600/1-79-012)
- Kullgren J, Hermansson K, Broqvist P (2013) Supercharged low-temperature oxygen storage capacity of ceria at the nanoscale. *J Phys Chem Lett* 4:604–608
- Le Gal A, Abanades S (2012) Dopant incorporation in ceria for enhanced water-splitting activity during solar thermochemical hydrogen generation. *J Phys Chem C* 116:13516–13523
- Lin F, Alxneit I, Wokaun A (2015a) Structural and chemical changes of Zn-doped CeO_2 nanocrystals upon annealing at ultra-high temperatures. *Cryst Eng Commun* 17:1646–1653
- Lin F, Delmelle R, Vinodkumar T, Reddy BM, Wokaun A, Alxneit I (2015b) Correlation between the structural characteristics, oxygen storage capacities and catalytic activities of dual-phase Zn-modified ceria nanocrystals. *Catal Sci Technol* 5:3556–3567
- Lindstrom K, Nordin J (1976) Gas chromatography-mass spectrometry of chlorophenols in spent bleach liquors. *J Chromatogr A* 128:13–26
- Morales-Torres S, Silva AM, Maldonado-Hódar FJ, Machado BF, Pérez-Cadenas AF, Faria JL, Figueiredo JL, Carrasco-Marín F (2011) Pt-catalysts supported on activated carbons for catalytic wet air oxidation of aniline: activity and stability. *Appl Catal B Environ* 105:86–94
- Moreno M, Bergamini L, Baronetti GT, Laborde MA, Marino FJ (2010) Mechanism of CO oxidation over CuO/CeO_2 catalysts. *Int J Hydrog Energy* 35:5918–5924
- Ovejero G, Sotelo JL, Rodríguez A, Díaz C, Sanz R, García J (2007) Platinum catalyst on multiwalled carbon nanotubes for the catalytic wet air oxidation of phenol. *Ind Eng Chem Res* 46:6449–6455
- Pal M, Bera S, Sarkar S, Jana S (2014) Influence of Al doping on microstructural, optical and photocatalytic properties of sol-gel based nanostructured zinc oxide films on glass. *RSC Adv* 4:11552–11563
- Pintar A, Besson M, Gallezot P (2001) Catalytic wet air oxidation of kraft bleaching plant effluents in the presence of titania and zirconia supported ruthenium. *Appl Catal B Environ* 30:123–139
- Qin J, Zhang Q, Chuang KT (2001) Catalytic wet oxidation of *p*-chlorophenol over supported noble metal catalysts. *Appl Catal B Environ* 29:115–123
- Ramasamy V, Vijayalakshmi G (2015) Effect of Zn doping on structural, optical and thermal properties of CeO_2 nanoparticles. *Superlattices Microstruct* 85:510–521
- Richardson SD (2007) Water analysis: emerging contaminants and current issues. *Anal Chem* 79:4295–4324
- Robinson T, McMullan G, Marchant R, Nigam P (2001) Remediation of dyes in textile effluent: a critical review on current treatment technologies with a proposed alternative. *Bioresour Technol* 77:247–255
- Vepsäläinen M, Kivisaari H, Pulliainen M, Oikari A, Sillanpää M (2011) Removal of toxic pollutants from pulp mill effluents by electrocoagulation. *Sep Purif Technol* 81:141–150
- Xia Y, Lin M, Ren D, Li Y, Hu F, Chen W (2016) Preparation of high surface area mesoporous nickel oxides and catalytic oxidation of toluene and formaldehyde. *J Porous Mater* 24:1–9
- Xu A, Yang M, Du H, Sun C (2006) Influence of partial replacement of Cu by Fe on the CWO of phenol in the $\text{Cu}_{0.5-x}\text{Fe}_x\text{Zn}_{0.5}\text{Al}_2\text{O}_4$ spinel catalysts. *Catal Commun* 7:513–517
- Yang S, Sun Y, Yang H, Wan J (2015) Catalytic wet air oxidation of phenol, nitrobenzene and aniline over the multi-walled carbon nanotubes (MWCNTs) as catalysts. *Front Environ Sci Eng* 9:436–443

Publisher's Note

Springer Nature remains neutral with regard to jurisdictional claims in published maps and institutional affiliations.